JMEPEG (2012) 21:1539–1551
DOI: 10.1007/s11665-011-0051-9

1059-9495/$19.00

Cavitation Erosion in Hydraulic Turbine Components and Mitigation by Coatings: Current Status and Future Needs

Raghuvir Singh, S.K. Tiwari, and Suman K. Mishra

(Submitted April 21, 2010; in revised form May 16, 2011)

Cavitation erosion is a frequently observed phenomenon in underwater engineering materials and is the primary reason for component failure. The damage due to cavitation erosion is not yet fully understood, as it is influenced by several parameters, such as hydrodynamics, component design, environment, and material chemistry. This article gives an overview of the current state of understanding of cavitation erosion of materials used in hydroturbines, coatings and coating methodologies for combating cavitation erosion, and methods to characterize cavitation erosion. No single material property fully characterizes the resistance to cavitation erosion. The combination of ultimate resilience, hardness, and toughness rather may be useful to estimate the cavitation erosion resistance of material. Improved hydrodynamic design and appropriate surface engineering practices reduce damage due to cavitation erosion. The coatings suggested for combating the cavitation erosion encompasses carbides (WC Cr_2C_3, Cr_3C_2, 20CrC-80WC), cermets of different compositions (e.g., 56W_2C/Ni/Cr, 41WC/Ni/Cr/Co), intermetallic composites, intermetallic matrix composites with TiC reinforcement, composite nitrides such as TiAlN and elastomers. A few of them have also been used commercially. Thermal spraying, arc plasma spraying, and high velocity oxy-fuel (HVOF) processes have been used commercially to apply the coatings. Boronizing, laser surface hardening and cladding, chemical vapor deposition, physical vapor deposition, and plasma nitriding have been tried for surface treatments at laboratory levels and have shown promise to be used on actual components.

Keywords cavitation, coating methods, coatings, corrosion, erosion, hydroturbine, steels

1. Introduction

Hydroturbine components, such as guide vane, runner blade, labyrinth, pivot ring, pump, compressor, etc., are known to be affected by cavitation or combination of cavitation, erosion, and corrosion, as illustrated in Fig. 1. Cavitation-led erosion/pitting may exceed 40-mm depth beyond which a hydroturbine runner is considered undesirable for operation and is generally taken out from the service for maintenance (Ref 1, 2). The cavitation penetration rate of critical components, such as impellor, turbine blade, and casing were found as high as 10 mm/year (Ref 1). Typical metal loss experienced by the turbine runner due to cavitation is reported to be 5 kg/m^2/10,000 h, and it is about 200 kg loss after a few years of operation (Ref 1). Trailing edge (of the size 800 × 250 × 8 mm) of a turbine blade lost about 40-60 kg of metal after 6000-8000 h of operation (Ref 2). A huge quantity of metal loss clearly indicates cavitation erosion as a serious problem particularly in the South Asian countries belonging to Himalayan regions (such as India, China, and Nepal) (Ref 3–5). One of the major causes of this is the presence of large contents of quartz (∼90% or 5000-20,000 ppm) in the silt (SiO_2, Al_2O_3, Fe_2O_3, MgO, CaO, etc.), particularly during monsoon season (Ref 6). Quartz which is known to have an extremely high hardness (7 on Moh's scale compared to 10 for diamond) can thus easily wear out the components in service. Thus, emphasis on the cavitation- and silt-assisted erosion is important for countries, such as India, Nepal, and China, as a major portion of hydropower in these countries is being produced from the Himalayan Rivers that contain excessive silt contents. The hydropower potential in India is estimated to be ∼120,000 MW from the Himalayan regions which is currently about 32,000 MW (Ref 7). Approximately 20% electricity is being generated worldwide from the hydropower, and the components used therein are highly susceptible to cavitation erosion. In New Zealand, approximately 80% of operational power stations are hydrostations (Ref 1). Canada, the largest power producer in the world, has more than 60% (>67,000 MW) power being produced from hydropower (Ref 8). The extent of cavitation erosion damage varies with the location of power stations and seasons, as they influence the silt contents in water. For instances, the cavitation erosion of the turbine at various power stations in India ranges from severe (needs repair after every two monsoon) to considerable damage (needs repair after every 7-8 monsoon) (Ref 9). The cavitation erosion-led damages, in recent times, have further aggravated due to increase in operational pressure, speed of hydraulic systems, and miniaturization of components to enhance the capacity of turbines (Ref 10).

Development and use of more resistant materials, application of coatings, modification of component's design, and minimizing silt contents in the water have been attempted to reduce the cavitation erosion. The micro-injection of bubbles (of non-condensable gases) to cover the component surface has

Raghuvir Singh, S.K. Tiwari, and **Suman K. Mishra**, Council of Scientific & Industrial Research-National Metallurgical Laboratory (CSIR-NML), Jamshedpur 831007, India. Contact e-mails: raghujog@yahoo.co.in and rsr@nmlindia.org.

Fig. 1 Runner blades showing cavitation erosive failure (Ref 6)

also been tried to combat the cavitation erosion. Among these, coatings/surface engineering appears most viable option to enhance the lifetime of the component. Extensive reviews addressing the physical and chemical processes involved with the cavitation erosion and response of materials have been presented earlier (Ref 11, 12). A few case studies related to the declined performance of hydroturbine components due to cavitation erosion have also been described (Ref 11, 12). This article reviews various coatings and coating methodologies developed to increase the cavitation erosion resistance. Brief discussion on various aspects of cavitation erosion, metallurgical properties related to cavitation, and methods to characterize cavitation erosion have also been presented. The newer and the future coatings to enhance the performance of underwater components have also been highlighted.

2. Some Aspects of Cavitation Erosion

2.1 Pure Cavitation

Cavitation erosion of equipment is remarkable consequence of cavitation together with the cavitation led vibrations and noise, which reduces the efficiency of power plants. Cavitation is a physical phenomenon which represents the formation, growth, and collapse of bubbles (Ref 13). It generally occurs in situations where high-velocity liquid flow encounters a pressure change. High fluid velocity in throttling area reduces the local pressure below the overall fluid vapor pressure resulting in the formation of vapor bubbles. The "cavitation number" (σ) is widely used to estimate the cavitating potential of flowing liquid and is generally expressed as:

$$\sigma = (P - P_v)/(1/2\rho V^2) \quad \text{(Eq 1)}$$

where P is upstream pressure, P_v is downstream pressure; ρ and V are density and velocity of liquid flow, respectively. Critical value of cavitation (σ_{crit}) can be determined for all types of equipment at specific hydrodynamic conditions; higher value of σ_{crit} indicates the likeliness of cavitation e.g., $\sigma > \sigma_{crit}$ implies occurrence of cavitation, and $\sigma < \sigma_{crit}$ implies no cavitation.

For nuclei to trigger to a cavity or bubble, it must be subjected under the tensile forces for sufficient time. Number of cavitation bubbles is proportional to the amount of tension (T), time (t) below the critical pressure, number, and size of the nuclei (Ref 14) i.e.,

$$\text{No. of bubbles} = f(T,\ t,\ \text{number},\ \text{and size of nuclei})$$

As bubble moves to high-pressure regions, it collapses with intense shock waves emerging from its center. It is the bubble collapse which is responsible for the erosion or loss of metal. The mechanism of cavitation erosion is though not yet clearly understood; the current understanding follows two explanations of cavitation erosion (Ref 15, 16). When a bubble collapses within the liquid volume (symmetrical collapse), a shock wave emanates to the surrounding liquid. However,, bubble in contact with or very close to the solid boundary collapses in asymmetrical fashion. Here, the cavity is perturbed from the side, away from the solid boundary, and finally the fluid penetrates through the cavity in the form of micro-jet. These mechanisms also lack explanation as shock waves are attenuated rapidly, and the radius of the cavity (micro-jet) is too small to cause the cavitation erosion (Ref 17, 18). The collapse of the cavity cloud may rather have more severe effect on the adjacent surface/solid boundary (Ref 19). The process of repeated collapsing of bubble cloud can induce a pressure as high as 1000 MPa, which is sufficient to bring about plastic deformation and consequent removal of metals/alloys (Ref 20). Plastic deformation, as a result of cavitation, is often evidenced by the undulations/deformation bands and pile ups in the underlying material. Early stages of cavitation have been well monitored and documented by Chen and Weite (Ref 21); they showed that the cavitation-induced plastic deformation and the pile up evolved along twin boundaries and surrounding the carbide (along grain boundaries) in Alloy 690. Interphase and grain boundaries in the materials are the preferred sites for deformation where failures initiate. Increase in deformations/dislocations were observed with the time of exposure to cavitation, which subsequently coalesced as cracks and resulted into the removal of material (Ref 21).

Cavitation erosion (in the absence of solid particles) is often predicted by measuring the impact energy of the bubble collapse (Ref 22). This is done with an assumption that only the cavitation impacts with the energy larger than a certain threshold level will cause the erosion of materials. Threshold impacts of the bubble collapse are important as they initiate fatigue fracture of the surface. Impacts due to collapsing of

bubbles are reported to correspond to the fatigue limit of the materials (Ref 23). The impact energy below such threshold cannot produce elastic or plastic deformation and hence no metal loss. Threshold levels of impact energy have been revealed experimentally for aluminum, copper, and resin by using cavitating jet at different conditions. The increase in impact energy (ΣF_i^2) has been shown to decrease threshold level to cause cavitation erosion (Ref 22). Hattori et al. measured the bubble impact load during collapse of bubble by using sensor at various standoff distances from the specimen surface as shown in Fig. 2 (Ref 24). They found impact energy to decrease with increase in standoff distance from the location of bubble collapse, as shown in Fig. 2. The erosion-affected area, therefore, remained up to a certain limited distance (a few micrometer) from the point of bubble collapse. Changes in ΣF_i^2 also correlated well with the mass-loss data; increase in ΣF_i^2 was reported to enhance the erosion rate as illustrated by the Fig. 3 (Ref 24)., In their study, they used vibratory test method to measure bubble impact and cavitation. Corresponding erosion rates (MDE) for various alloys such as stainless steel and aluminum vary linearly with the impact energy (e) (Fig. 3) and is related as given by (Ref 25):

$$e = \Delta T/\rho c \times F_i^2 \quad \text{(Eq 2)}$$

where ΔT is holding time and considered to be a constant irrespective of impact load, ρ is density of the test liquid, c is the velocity of sound in liquid, and F_i is impact load.

The cumulative impact energy E (i.e., Σe) is given as

$$E \propto \Sigma F_i^2 \quad \text{(Eq 3)}$$

where ΣF_i^2 is calculated as $\Sigma(F_i^2 \times n_i$, n_i being number of impacts).

2.2 Solid Particle-Assisted Cavitation Erosion

In most practical situations, cavitation erosion is assisted by the solid particles present in the liquid media. This results into much higher erosion rate than the sum of erosion due to silt and liquid separately. It is often referred to as the synergetic erosion (Ref 26, 27). Figure 4 clearly demonstrates and differentiates the damage of Peltron turbine needle due to pure sand and combined effects of sand and cavitation erosion (Ref 27). The needle under the combined effect of cavitation and sand erosion shows much deeper and severe attack as compared to the cavitation only. Nanda (Ref 28) reported that the medium silt content (in the water) causes 4 times higher erosion than the cavitation in clean water (without silt), and the combined effect of cavitation and erosion is 16 times higher than cavitation alone. The particle entrainment in the cavitating medium increases the concentration of bubble nuclei and consequently promotes the occurrence of cavitation. A 10-15% increase in the incipient cavitation number (bubble nucleation) was

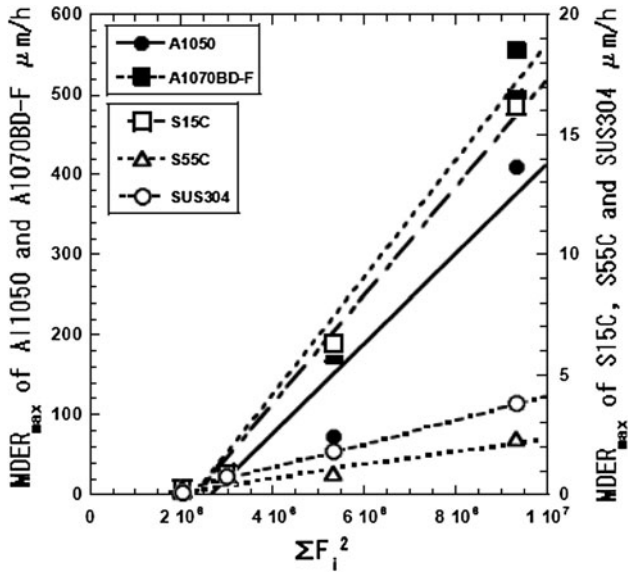

Fig. 3 Change in erosion rate with increase in impact energy (ΣF_i^2) (Ref 24)

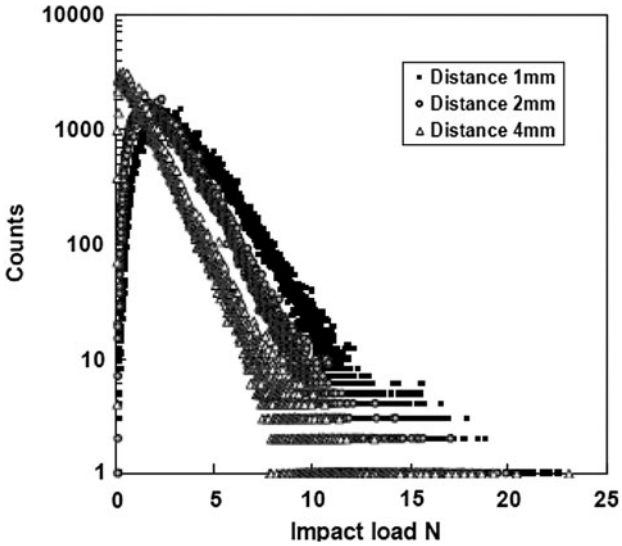

Fig. 2 Impact load due to bubble collapse at various standoff distances from the specimen surface (Ref 24)

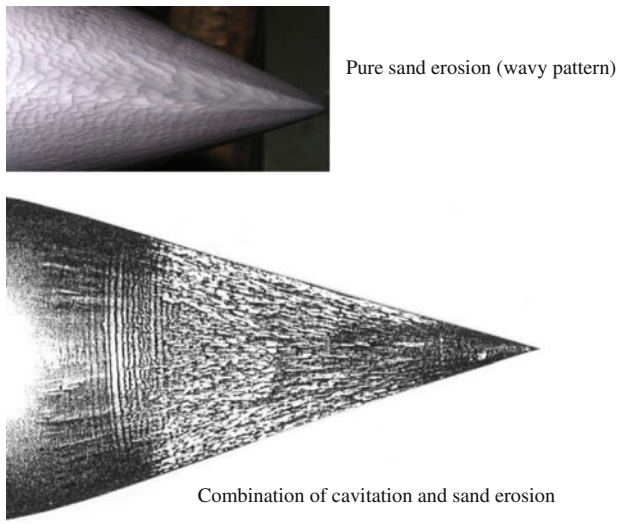

Fig. 4 Damage in Peltron turbine needle due to pure sand and combined effect of sand and cavitation erosion (Ref 27)

reported by Toshima et al. (Ref 29) in silt-laden water as compared to the tap water. Cavitation erosion in presence of solid particles is further dependent on the impingement angle and properties including the shape, size, and hardness of the erodent. The effect of incidence angle of the erodent on the variation of erosion rate of brittle and ductile material is illustrated in Fig. 5. The ductile materials are susceptible to erosion at relatively low impingement angles as opposed to the brittle materials which are eroded severely at relatively larger angles. Particles impinging at angles $>90°$ cause low-cycle fatigue and accumulation of plastic deformation that promotes material detachment. On the other hand, at low angles ($<90°$) micro-cutting governs the material damage (Ref 30). For ductile materials, the shape and kinetic energy of erodent are the most important factors to determine the erosion rate (Ref 31), while, for brittle materials, the erosion rate is caused by kinetic energy, particle size, hardness, and toughness of the erodent (Ref 32). Micro-model on the silt-accelerated erosion suggests that the micro jet, from the collapsing of bubble, actually enhances the velocity of solid particle much higher than the flow rate (in the absence of bubble) (Ref 33). Further, the solid particle within the cavity gains the drag forces and torque, by the micro jet that initiates micro-cutting action. Erosion is often correlated to the velocity of solid particle as erosion P velocity^n, where the value of exponent "n" varies with material and other operating conditions. Researchers have worked out the values of 'n" for various materials; for instance, Truscott (Ref 34) showed it to be 1.7 for steel; Zhang et al. (Ref 35) showed it to be 3-4.5 for non-metallic coatings. Similarly, Arnold and Hutchings (Ref 36) found the velocity exponent for elastomers between 2.9 and 5.1 at impingement angles ~30° and 90°, respectively. Bjordal et al. (Ref 37) observed erosion rate to depend upon the particle flux rate (i.e., concentration of impacting particles per unit area on the specimen) and showed it to be related as erosion rate P concentration$^{0.25\text{-}1.27}$ for different metals and coatings. The exponent value was close to 1 for most of the materials when tested for longer periods.

Several models have dealt with the erosion in the liquid in presence of solid particles, such as for silt erosion conditions. Bardal (Ref 38) described the most general formula for pure erosion as

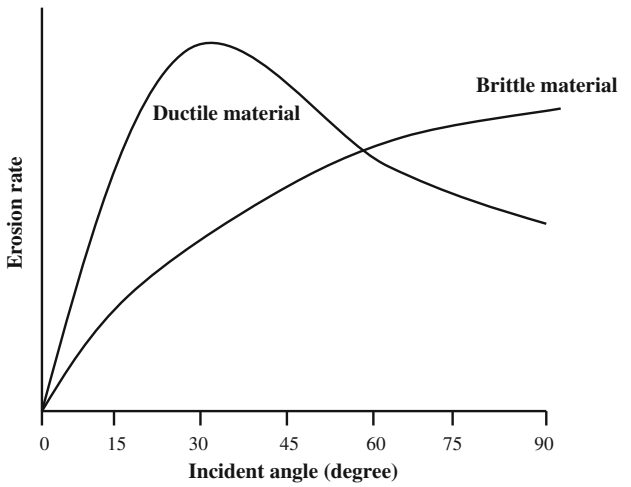

Fig. 5 Effect of incidence angle of erodent on erosion rate of brittle and ductile material

$$W = K_{\text{mat}} K_{\text{env}} c V^n f(\alpha) \quad \text{(Eq 4)}$$

where W is erosion rate in mm/year, K_{mat} is material constant, and K_{env} is constant depending upon environment, c is concentration of particles, and $f(\alpha)$ is the function of impingement angle, V is velocity of particle, and n is the exponent of velocity.

Truscott (Ref 34) presented following equation to predict the cavitation erosion of a pump assuming sliding of spherical particle over the surface of pump:

$$\text{Erosion} \propto (\rho_p - \rho) d^3 p K \left(V^3/D\right) \quad \text{(Eq 5)}$$

where V is the characteristic velocity of liquid, D is the characteristic dimension of the machine, ρ_p is density of particle, d is diameter of particle, p is number of particles per unit surface area, ρ is density of the liquid, and K is experimental coefficient depending upon the nature of abrasive. This equation is proportional to the experimental coefficient which is dependent on the abrasive nature of particles. Tsuguo (Ref 39) showed an empirical equation for cavitation erosion of turbine, based on the erosion data obtained (over the 8 years of time) from 18 hydropower plants. It was based on the uniform thickness loss of material and expressed as follows:

$$W = \beta C^x a^y k_1 k_2 k_3 n y x V^n \quad \text{(Eq 6)}$$

where β is turbine coefficient at the eroded part, C is the concentration of suspended sediment, and V is relative velocity. The term a is average grain size coefficient on the basis of unit value for grain size ~0.05 mm. The terms k_1 and k_2 are the shape and hardness coefficients of sand particles, respectively, and k_3 is abrasion-resistant coefficient of material. The x, y, and n are exponent values for concentration, size coefficient, and velocity, respectively. The values of x and y are close to the unity; any deviation in linear proportionality is determined from the plot of wear versus parameter.

2.3 Electrochemical (Corrosion)-Assisted Cavitation Erosion

The cavitation erosion is aggravated by the electrochemical reaction occurring on the alloy surface. The repeated bubble formation and collapsing may cause the rupture of electrochemically formed protective passive film which is generally responsible for the corrosion resistance of metals/alloys. The aggressiveness of the electrochemical reaction, however, depends upon the pH, concentration of corrosives (e.g., Cl^-), fluid flow, and pressure. At low fluid velocity, the passive oxide/scale remains intact to the surface but may be washed/swept away at relatively higher velocities and surface may appear clean. Corrosion in some situations is found to be an underlying cause of the damage of turbine components which could be the consequence of cavitation (Ref 40, 41). It has been reported that the corrosion-assisted erosion or combined erosion-corrosion is a serious concern in offshore industries (Ref 42). Various interactive zones among cavitation, erosion, and corrosion are well represented by the schematic shown in Fig. 6 (Ref 42). The total erosion loss due to various mechanisms is expressed as follows (Ref 43):

$$W_{\text{Total}} = W_{\text{erosion}} + W_{\text{corrosion}} + \Delta W_{\text{erosion}} + \Delta W_{\text{corrosion}} \quad \text{(Eq 7)}$$

where $\Delta W_{\text{erosion}} + \Delta W_{\text{corrosion}}$ is synergy. $\Delta W_{\text{corrosion}}$ is erosion-enhanced corrosion, and $\Delta W_{\text{erosion}}$ is corrosion-enhanced erosion. The effect of cavitation is included in the $\Delta E_{\text{erosion}}$ as mechanical synergy.

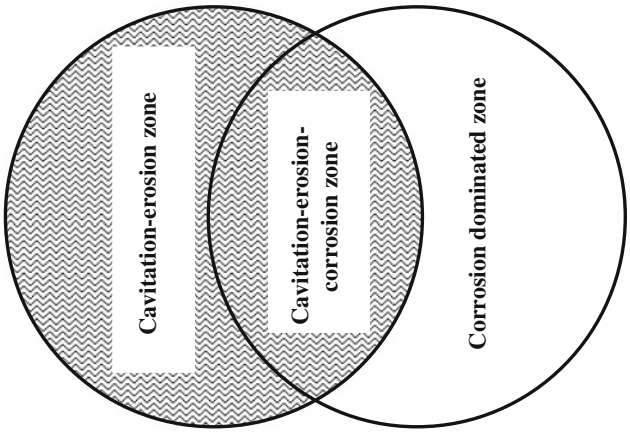

Fig. 6 Various interactive zone among cavitation, erosion, and corrosion

3. Cavitation Erosion-resistant Alloys for Hydroturbine

Although great efforts have been made to develop the cavitation-resistant materials and improve the hydroturbine design, the problem of cavitation/silt erosion yet remains unsolved. Martensitic stainless steels (such as 13Cr-4Ni, 13Cr-0.5Ni, manganese steels) are, by far, the most popular choices for fabricating turbine components where cavitation erosion is primary concern. For instances, runner blades are fabricated from 13Cr-1Ni, 13Cr-4Ni, 16Cr-5Ni, and 18Cr-8Ni stainless steels (Ref 44); guide vanes and labyrinth (rotating) seal are made from 13Cr-4Ni, and 16Cr-5Ni; and labyrinth (stationary) seal from nickel aluminum bronze (JM7) alloy. The martensitic stainless steels possess higher cavitation erosion resistance than the austenitic, while the ferritic stainless steels have the lowest resistance (Ref 45). It has been observed that the cavitation erosion of martensitic stainless steels increases with increase in the hardness (Ref 46). DIN 4112 (Fe, 18.5% Cr, 1.15% Mo, 1% Mn, 1% Si, and 0.91% C) shows higher cavitation erosion resistance than the BS 431S29 (Fe, 15.6% Cr, 2.34% Ni, 1% Mn, 0.8% Si,and 0.11% C) for similar heat-treatment conditions. This is due to the difference in the carbon content and to a lesser degree, the chromium content (Ref 42). Carbon in the alloy has both positive and negative effects on cavitation erosion resistance. High carbon content in DIN 4112 shows high hardness of its martensitic matrix, but it increases the formation of the coarse chromium carbides that provide sites for the initiation of erosion damage (Ref 46). The NiTiNOL (Ni-55%, Ti-45%) has also been suggested as an alternative material for components of turbine as it offers high fatigue resistance and mechanical properties (Ref 46). The martensitic phase in NiTiNOL has good damping characteristic and provides self-accommodating twinned structure. High cost of this alloy may, however, restrict its use as turbine components. The surface alloying or cladding of NiTiNOL on stainless steels, using high-power lasers, may be an alternative choice to reduce the cost of component. Iron-based alloy (CaviTech) containing alloying elements, such as cobalt, chromium, and manganese (altogether to the maximum of 9%) has been developed, which has demonstrated significantly high cavitation erosion resistance (Ref 1).

4. Dependence of Cavitation Erosion Resistance on Various Metallurgical Properties

Material damage due to cavitation erosion is dependent on the cavitation intensity of the medium, erodent properties, and resistance of the materials to cavitation. Cavitation resistance is not precisely a definable property of material. One-to-one correspondence, therefore, with any independent measurable metallurgical property has not been reported. It is generally postulated that the cavitation erosion resistance is high for the materials which contain lower stacking fault energy, as they can undergo easier planar slips formation (Ref 47) and stress induced phase transformation (Ref 48). Such materials have high work hardenability, and good elastic properties with homogeneous small-grained structure such as Stellite (Ref 49). An excellent cavitation resistance of cobalt-based alloys is well known since the early 1970s (Ref 1). The key microstructural factor for these alloys is the fine deformation twins accompanied by the cavitation-induced phase transformation. Martensitic stainless steels have also demonstrated high cavitation erosion resistance; they, however, have certain drawbacks such as susceptibility to intergranular corrosion that can enhance the rate of cavitation erosion (Ref 50). Such stainless steels are generally used in the tempered condition. Tempering of martensitic stainless steel causes the intergranular chromium carbide precipitation which reduces the erosion resistance (Ref 50). Investigations showed that the maximum susceptibility to intergranular corrosion is observed in steel tempered in the temperature ranges 500-600 °C. Tempering the stainless steel at >600 °C reduces sensitization to the lowest level or avoids it completely. Early statistical research pointed out hardness as a primary correlation factor and showed that the increase in hardness reduces the cavitation resistance (Ref 51–53). This, however, is contradicted by several other researchers who concluded that hardness or the strength/toughness alone cannot represent the cavitation resistance of materials (Ref 54–57). Competing theories involved a few other mechanical properties, such as combination of ultimate tensile strength and elastic modulus (ultimate resilience) (Ref 54), the combination of ultimate resilience and hardness (Ref 55), energy absorption characteristics (Ref 56), and fatigue strength (Ref 57) to represent the cavitation resistance in a better manner. Ultimate resilience is the combined material property shown by the area under the triangle obtained by raising the yield point to the level of ultimate tensile strength. Based on these, following mathematical formulations have been proposed and reported (Ref 54–56):

$$\text{Ultimate resilience (UR)} = (\text{UTS})^2/2E \quad \text{(Eq 8)}$$

$$\text{Modified ultimate resilience (MUR)} = (\text{UTS} \times \text{Hardness of substrate})/2E \quad \text{(Eq 9)}$$

$$\text{Composite modified resilience (CMR)} = (\text{UTS of substrate} \times \text{Hardness of coating})/2\,\text{Young modulus of substrate} \quad \text{(Eq 10)}$$

Higher value of the above parameters indicates greater resistance of materials against cavitation erosion. Contradictions to the above correlations were also quite common. For instance, borided 13Cr-4Ni stainless steel though showed the higher UR $\sim$3.6 J/cm^3 than the base 13Cr-4Ni (1.9 J/cm^3), it

did not produce the highest cavitation resistance (Ref 58). It was rather reported to be dependent upon the strain energy. The base 13Cr-4Ni with the highest strain energy ~112.1 J/cm^3 showed better cavitation resistance than the borided + tempered (64.7 J/cm^3) and borided alone (6.3 J/cm^3) (Ref 58). Materials with lower grain sizes and higher mechanical properties exhibited better cavitation resistance (Ref 59). Nanomaterials or nano-crystallite structures can enhance the cavitation erosion resistance as they possess good plastic properties with the hardness higher than the conventional materials. Materials containing the grain size below 100 nm are generally called nanomaterials, although the grains (crystallites) smaller than 20 nm are preferred (Ref 60, 61) to achieve special properties. Higher grain boundary area in the fine grained than in the conventional materials is the reason for special properties. For instance, 50% of the volume is occupied by the grain boundaries in a material containing 5 nm grains (Ref 62). In the materials with larger grain boundary percentage (nanomaterials), grain boundary sliding acts as a main deformation mechanism unlike dislocations in the conventional materials. If grain size is too small (below 15 nm), then the grain boundary sliding causes the decrease in hardness, although, it improves the stretching, and hence, the reduction in erosion resistance of materials.

5. Surface Engineering and Coatings for Preventing Cavitation Erosion

To overcome cavitation/erosion related failures, three approaches have generally been considered: optimization of hydraulic design of the components, development of a new cavitation-erosion-resistant alloy, and coatings of the components. Cavitation-free geometry may also become susceptible to erosion damage if a surface roughness is increased by the abrasive effects of sand. Higher roughness on the surface generally enhances the cavitation intensity and erosion of the solid surface. The hydraulic design and a new alloy development are beyond the scope of objective of the present review. The study that has been carried out on coatings and surface engineering to improve the cavitation/erosion resistance, and is available in the literature, has been discussed in the forthcoming sections.

5.1 Coating Systems for General Cavitation and Erosion Resistance

Among various coating systems, hard metallics, intermetallics, carbides, borides, oxides, carbonitrides, metal-ceramic (cermets), silicides, and non-metallic materials have been widely used for cavitation erosion resistance. Such coatings are produced either by reinforcing the ready-to-use coating materials or in-situ fabricated coating (by mixing various powder precursors in the preferred ratio) by using suitable heat source. Hard chromium coatings have been used to enhance the wear/abrasion and cavitation resistance of components belonging to earthmovers, mining, transport systems, and mould for plastics. Metal nitrides such as TiN, CrN, etc. have been modified to the multi component (e.g., TiAlN, TiCN) and multilayer coatings (e.g., TiN/TiAlN) for various engineering components. Multilayer coatings offer multifunctional characteristics, such as low residual stresses, good adherence to substrate, improved hardness to toughness ratio, and low friction coefficient (Ref 63). The mechanism of deterioration of coating in multiple phases, however, is very complex. Increase in the number of coating layers will increase the physical interphase boundaries (weak sites) which may become the preferred sites for failure (either mechanical or corrosion) to originate. Performance of the coatings during fluid flow shows dependence on several parameters, such as ratio of the size of coating particles to the erodent, relative hardness, shape of the erodent, and conditions of the flow (Ref 64). The latest generation of coatings are represented by the nanocomposites (such as TiN + DLC) and lubricating coatings to improve the surface tribology. Cermets, such as WC, Cr_2C_3, and Cr_3C_2 particles, embedded in a metal binder (a pure metal or a mixture consisting of Ni, Cr, and Co) are widely used to improve cavitation, erosion, and corrosion resistance of stainless steels (Ref 65). Carbides with more than one binder matrix, such as WC-CrNi, WC/CrC-CoCr, and NiCrSiFeC are increasingly used to tailor high cavitation, abrasion, and corrosion-resistant surfaces (Ref 37, 66). Partial or complete substitution of WC by Cr_3C_2 in the NiCr-type corrosion-resistant matrix, using HVOF method, showed better tribological properties (Ref 66). It has been reported that the erosion mechanism of the cermet coatings is controlled either by the carbide particles (such as in WC-Cr_3C_2-Ni, Cr_3C_2-NiCr) or metallic binders (such as in WC-Co, WC-Co-Cr). In situations where binder matrix is highly corrosion resistant (such as Cr_3C_2-NiCr), erosion occurs by the removal of carbide particles due to impact. In case of a low resistant binder (such as in WC-Co), it corrodes and loosen the carbide particle that results into the erosion of the material. This has also been supported by Toma et al. (Ref 65) who found the best erosion-corrosion resistance of HVOF sprayed Cr_3C_2-NiCr coating due to its high corrosion-resistant matrix (NiCr). They assessed and compared the erosion resistance of several coatings by using solid particle erosion method. The size of the silica particles used for this purpose was in the range between 100 and 500 μm and they were blown at the rate of 100 g/L. The results of this investigation are shown in Table 1 (Ref 65). The cavitation erosion resistance of AISI 316 stainless steels was shown to improve significantly with the ceramic powders reinforced by the laser heating source (Ref 67). The CrB_2 and WC coatings enhanced the cavitation resistance of as-received AISI 316 by about 9.4 and 8.5 times, respectively. The increase in the cavitation resistance obtained by using Cr_3C_2 and SiC was observed by a factor of 4.8 and 2, respectively (Ref 67). The TiC and Cr_2O_3 have neither improved nor reduced the cavitation resistance of stainless steel (Ref 67). The hard particle-matrix interphase is weaker location and is found vulnerable to corrosion and erosion. Also such zones of phase difference undergo preferential corrosion due to formation of galvanic coupling between the two phases.

Laser cladding of AISI 420 (martensitic stainless steel) with NiAl-Ni_3Al intermetallic composites (IC) and intermetallic matrix composites (IMC) with TiC reinforcement was reported to enhance the cavitation resistance of the substrate by 3.3 and 3.6 times, respectively (Ref 10). The improvement by laser cladding has been attributed to the high work hardening ability of the nickel aluminide coating. The cavitation resistance was further improved by strengthening the matrix with TiC reinforcement. No correlation was, however, found between erosion resistance and hardness over a range of process parameters studied. This indicates that the hardness alone cannot improve the erosion resistance of materials (Ref 10).

Similar coatings containing Ni and Al, applied by using the cathode arc plasma (CAP) and ion plating processes were reported to improve the cavitation resistance of AISI 1045 carbon steel, in 3.5% NaCl and HCl solutions, by 10 and 2.5 folds, respectively (Ref 68). Laser melting of NiTi powder, applied by the plasma spraying, has been attempted to enhance the cavitation erosion resistance of Ti6Al4V alloy (Ref 68, 69). The mixture of 62% Ni and 38% Ti powders sprayed on surface of Ti6Al4V was remelted at $>6 \times 10^8$ W/m^2 power density using high-power laser. The cavitation resistance of thus cladded titanium alloy was observed to increase by 380 folds.

5.2 Coating Systems for Silt Erosion and Cavitation in Hydroturbine Components

The most preferable characteristics of a protective coating under heavy silt conditions are (i) cavitation resistance, (ii) abrasion resistance, (iii) strong bonding to the substrate, (iv) corrosion resistance, (v) vibration damping, and (vi) easy applicability at the site. Surface boriding is a hardfacing process frequently used for improving the sliding and abrasive wear behavior of low alloy and chrome-moly steels, and cobalt alloys. Boronization of hydroturbine steel (13Cr-4Ni) has shown varied cavitation resistance, and often depends upon the post boronizing treatment or on the state of base substrate (Ref 58, 70). The boronization of 13Cr-4Ni stainless steel, performed by pack cementation technique, has shown to reduce the cavitation resistance drastically, despite attaining a high coating hardness (~750 HV). Tempering of the borided component at 600 °C though improved the cavitation resistance; it yet remained below the untreated 13Cr-4Ni steel (Ref 58). Improvement in cavitation resistance on tempering 13Cr-4Ni seemed due to the retention of the reverted austenite on cooling (Ref 58). The failure has been attributed to extremely brittle nature of the coating, reduction in elongation (from 14.8 to 0.8%) and lower strain energy (1/19th of the as receive alloy) as compared to the bare 13Cr-4Ni. The coarse microstructure of steel produced as a result of boriding is reported to cause the brittle failure (Ref 58). In a comparative study that encompassed various coatings including boronizing (by pack cementation), the highest cavitation erosion was exhibited by the borided T410 martensitic stainless steel (Ref 9) (Table 2). The borided 13Cr-4Ni stainless steel was found to have cracks which were responsible for enhanced volume loss under the high impact energy. On the other hand, boriding of hydraulic valve made from AISI 440C stainless steel showed excellent performance (Ref 70). Under various ASTM test conditions, boron carbide (B_4C) with the highest hardness showed better erosion resistance than the tungsten carbide/cobalt (Ref 71); whereas tungsten carbide/cobalt with the highest toughness showed better abrasion resistance than the boron carbide. It was concluded that the combination of hardness and toughness in the composite carbide coating led to the superior performance of steel against both erosion and abrasion. The wear resistance of various coatings studied is shown in Table 3 (Ref 71).

Table 1 Performance of various hard coatings (Ref 65)

	Corrosion rate, mm/year			Erosion-corrosion rate, mm/year	
	NaOH	H_2SO_4	Sea water	NaOH	Sea water
WC-Cr_3C_2-Ni	0.38	0.15	NA	0.4	NA
Cr_3C_2-NiCr	0.17	0.077	NA	0.17	NA
WC-Co	NA	NA	0.76	NA	1.6
WC-Co-Cr	NA	NA	0.32	NA	0.55
Cr_2O_3-Al_2O_3-TiO_2	3.16×10^{-5}	3.64×10^{-4}	NA	0.27	NA
Cr_2O_3	7.6×10^{-4}	1.5×10^{-3}	NA	0.35	NA

Erosion-corrosion tests are performed using 100 g/L silica sand grain size varying from 100 to 500 μm added to the solution of NaOH and sea water, test duration ~48 h, temperature ~20 ± 2 °C; 'NA' indicates not available

Table 2 Properties and erosion resistance of 13Cr-4Ni stainless steel 'as received' and after boriding, nitriding, and with ceramic coating (Ref 9)

Materials steel/coatings	Density	Microhardness, HV	Coating thickness, μm	Volume-loss mm^3/cm^2/kg of erodent
13Cr-4Ni steel as grounded	7.8	288-300	…	1.38
13Cr-4Ni steel plasma nitrided	7.8	1000-1050	200-250	1.39
13Cr-4Ni steel borided	7.1	1650-1700	50-60	0.90
13Cr-4Ni steel hard chrome plated	7.14	700-750	50-60	1.28
13Cr-4Ni steel D-gun sprayed WC + 12Co	12.5	1100-1150	200-250	0.77
13Cr-4Ni steel D-gun sprayed Cr_3C_2 + 25NiCr	6.25	750-800	200-250	2.39
T410 steel borided	7.1	1950-2000	50-60	0.33

Test conditions. Erodent size and shape: 80-170 mesh mean particle size 135 μm of irregular shape; erodent type: mineral sand of hardness 1100 HV; erodent concentration and flow rate: 2000 ppm and 40 g/min; water velocity and flow rate: 75 m/s and 20 l/min; water temperature: inlet 28 °C and outlet 47 °C; chamber pressure: 330 mm of water column; experimental error: ±3.2%; wear rate measurement error: ±0.5%; impact energy: 10.5 μJ based upon mean particle size; specimen size: 12.76 ϕ = 12.76 mm long. Impact energy 1/2 $mv^2 = \pi\rho d^3 v^2$, where m is the mass, ρ the density, v the velocity and d is the diameter of the particles

Table 3 Wear results of B_4C, WC/6% Co, and WC/MO_2C coating evaluated by various ASTM methods (Ref 71)

Material	B_4C	WC/6% Co	ROCIEC100 (WC/Mo_2C)
ASTM G76: 200 μm SiC, $cm^3\ g^{-1}$	1.4×10^{-5}	1.3×10^{-4}	3.2×10^{-6}
200 μm erosion profile, $cm^3\ g^{-1}$	1.3×10^{-5}	NT	3.1×10^{-6}
ASTM G76: 50 μm SiC, $cm^3\ g^{-1}$	5.6×10^{-6}	1.6×10^{-4}	4.1×10^{-6}
ASTM G65, cm^{-3}	115	450	600
ASTM B611, cm^{-3}	13	28.7	1476.9

Cermets which are also among the most commonly used coating precursors to increase the cavitation or wear resistance generally contain WC, Cr_3C_2, Cr_2O_3, etc. with various metal binders. A Cr_3C_2 coating has lower wear resistance but higher fracture toughness than the WC-Co-based coatings (Ref 63). Mann and Vivek (Ref 72) have shown that the WC coating on 13Cr-4Ni stainless steel, applied by HVOF process, did not really improve the erosion resistance, during droplet erosion test. The coating was removed in a layer-wise manner during the test. Sugiyama et al. have carried out slurry erosion test on various cermets-coated martensitic stainless steel (SCS6) by using HP/HVOF process (Ref 73). The 20CrC-80WC coating, obtained by using combined HP/HVOF spraying, has shown the improvement in erosion resistance (by 86-143 times) followed by arc-sprayed 56W_2C/Ni/Cr (6-9 times), and spray-fused 41WC/Ni/Cr/Co coating (9 times) (Ref 73). The cavitation resistance of coatings was found to be affected by the number of pores present in the coating regardless of hardness. The coating with smaller pore density produced better results as compared to the larger pore density. The erosion rates recorded were found to be lower at the slurry impingement angles lower than 60° and increased between 60-90°. Plasma nitrided steel, in another study, showed poor abrasive and erosive wear resistances because of their lower microhardness values than the erodent hardness (<1100 HV of mineral sand) (Ref 74). Among the two different steels subjected to plasma nitriding, 12Cr performed much better than the 13Cr-4Ni steels. Hard chrome-plated steel has been identified as a potential erosion shield for I.D. fan blades of thermal power plants (Ref 75). The WC/Co in Fe-Cr-Ni matrix (E-C 29123) and T 35MXC (Al_2O_3-reinforced high-carbon steel) has been deposited by the oxy-fuel powder (OFP) and wire arc spraying (WAS) methods, respectively, onto the AISI 304 steel (Ref 30). Performance of these coatings were evaluated by slurry erosion method (slurry being the mixture of distilled water and 10% quartz particles with mean diameter in the range 200-300 μm) and compared with CA6NM (martensitic stainless steel) and AISI 431 stainless steels which are used for turbine components (Francis hydraulic turbine) (Ref 30). Coated stainless steels have performed better than the uncoated CA6NM and AISI 431 as shown in Fig. 7 (Ref 30). The better performance of T35 MXC and WC/Co in E-C29123 coatings have been attributed to their high hardness and Young modulus, respectively. The wear mechanism on the coated steel was observed to change from micro-cutting of matrix to spalling of the hard phases (Al_2O_3 in T 35MXC and WC in E-C29123) with increase in test duration (Ref 30).

Laser hardening of the martensitic stainless steels has been shown to produce better erosion resistance than the steel with hard carbide coatings during droplet erosion test (Ref 72). The laser-hardened AISI 440 martensitic stainless steel showed three-fold increase in cavitation resistance as compared with the base substrate (Ref 76). The higher cavitation resistance has been attributed to the higher content of retained austenite and precipitation of finer carbides during intense laser heating. Improvement in cavitation resistance of AISI 420 martensitic stainless steels is also reported by the laser melting (Ref 77). This has been attributed to the higher retained austenite (89%) and hardness (450 HV) than the as-received steel (220 HV) (Ref 77). A technology has been developed for laser transformation hardening of leading edge of steam turbine (LP) blades, by using CO_2 laser, which was subsequently put in service (Ref 78).

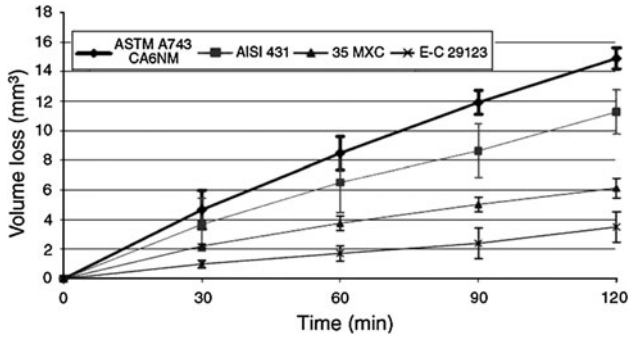

Fig. 7 Effects of various coatings on erosion loss of stainless steel 304 and uncoated ASTM A743 and AISI 431 alloys (Ref 30)

Alternatively, non-metallic coatings have been tried out by several researchers to improve the cavitation resistance of hydroturbine components (Ref 34, 79, 80). Nuttall (Ref 80), has observed 10 times better erosion resistance of polyurethane elastomers than that of the cast iron containing flaky graphite. Basu et al. (Ref 79) have also supported a good cavitation resistance of polyurethane coatings. Epoxy resin coatings applied on the axial pumps, impellers, and a Francis turbine runner showed satisfactory performance under abrasive conditions; contradictory conclusions, however, have been drawn by the other authors (Ref 34). Zhang et al. have studied the abrasion and combined abrasion-cavitation of five different polymer coatings selected from three generic classes, such as epoxy, nylon, and polyurethane elastomers (Ref 35). The epoxy resin reinforced with synthetic corundum particles and castable polyether-based polyurethane rubber demonstrated the most resistant behavior to both abrasion and combined abrasion-cavitation damage (Ref 35). Corundum particles reinforcement enhanced the resistance of the epoxy resin to erosion damage by more than 10 times, primarily due to increase in hardness of the resin matrix. It was also noticed that the polyurethane with high elasticity has the highest resistance to cavitation, while a brittle epoxy resin has the lowest resistance in high-silt-content water. Cavitation resistance of the epoxy coating has been shown to improve by modifying the epoxy with liquid rubbers, thermoplastics, and elastomer powder fillers (Ref 81).

6. Existing Coating Methodologies for Cavitation Erosion

Several advanced surface engineering techniques, such as plasma nitriding, chemical vapor deposition (CVD), physical vapor deposition (PVD), detonation gun, flame spraying, HVOF, laser cladding, and hardening have been used to modify the surface properties of engineering materials at laboratory level. Each of these methods produces different coating characteristics, such as microstructure, adhesion, bond strength, and hardness. The application of specific surface engineering technique depends upon the ease of equipment handling, coating precursor, portability of equipments at site, and geometry of the work piece. It is evidenced from the literature that not many technologies are available to engineer/coat the surface of components related to hydroturbine. Out of a few known methods, thermal spray-based methods, such as arc plasma spraying (APS), detonation gun, and HVOF have been commercially used on components of turbine to improve the cavitation erosion resistance. In detonation gun process, acetylene and oxygen gases are mixed into the barrel. Detonation using spark generates waves of high temperature and pressure, which causes melting of the powder particles. Particle velocity of the order of 750 or 1000 m/s (super D gun) can be achieved by changing certain parameters (Ref 66). The coating with high bond strength and minimum porosity can be produced by a detonation gun method. Coating thickness of 50-500 μm can be achieved by using this process. In HVOF process, fuel mixture (such as propane, propylene, hydrogen, or acetylene) and oxygen are burnt in the chamber. Powder introduced axially is melted and accelerated at a high velocity (600-1200 m/s) over the work piece. It provides sufficiently high coating adhesion (>70 MPa) to the substrate surface. There are, however, certain disadvantages of thermal spray processes such as oxidation and decomposition of the powder or wire feed stock which can affect the overall quality and composition of the finished coating. Carbides or cermets during plasma spraying are decomposed and subsequently react with the metallic binder due to high temperature of plasma flame. The decarburization of WC followed by the formation of unpreferable carbides such as W_2C, complex Co-W-C, and metallic tungsten often takes place during plasma spraying in the oxidizing atmosphere. HVOF spray process, as compared to detonation gun (~4000 °C) and arc plasma (~7000 °C), results in less frequent phase change due to lower flame temperature (~2700 °C). The HVOF process also produces relatively dense coatings (Ref 65). Microstructure of a spray coating is usually inhomogeneous. Discontinuities, such as pores, oxide lamellas, or incomplete, molten spray particles remain in the sprayed coatings. Thermal spray coatings have very limited strain to fracture, even if the coatings are made from pure metals which are normally expected to be very ductile (Ref 65). Coatings produced by thermal spray contain residual tensile stresses which can lead to cracking or spalling of the coating. Laser heating source has recently shown promise in producing cavitation-resistant surfaces (Ref 10, 67, 69, 82). It has been used for melting or hardening the outermost surface and cladding with hard powder (metallic/ceramic) particles. Laser surface melting of the martensitic stainless steels dissolves the large carbides, produces refined microstructure, and homogenizes the chemical composition (Ref 83, 84). This leads to improvement in hardness, toughness, wear resistance, and corrosion resistance of steels (Ref 83, 84). In a laser-hardened martensitic stainless steel, the volume of retained austenite improves the behavior of the modified surface against erosion. Retained austenite up to 10% has been found to increase the wear resistance of T410 steel (Ref 85). In another report, retained austenite up to 20-25% increased the rolling fatigue life of the bearing steel by 11.3 times (Ref 86). Various ceramic or alloy powders can be laser cladded on the surface of a component to enhance cavitation resistance. Commercial application of laser cladding to obtain better erosion and tribological properties are being increasingly used. A few such applications, on various components, made by the different industries are listed in Table 4 (Ref 78, 82). A typical laser-cladding process is shown schematically in Fig. 8. The laser source, powder feeder, and a device for specimen manipulation are put together for cladding or laser alloying purpose. Laser cladding can produce good metallurgical bonding between the coating and surface of the substrate, contrary to mechanical bonding evolved from various other coating methodologies. A significantly thick 1-3 mm clad layer can be fabricated by laser

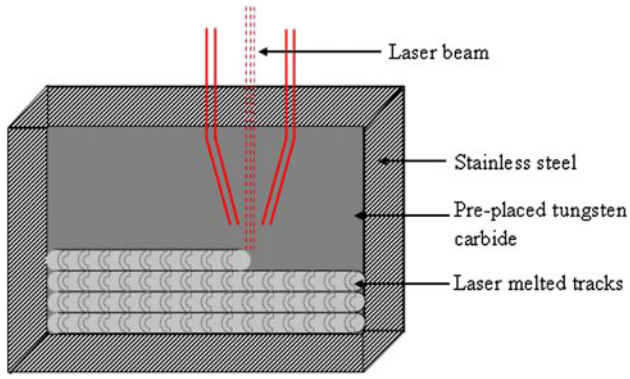

Fig. 8 Diagram showing the laser surface cladding method

Table 4 Commercial application of laser cladding on various components

Laser cladded components	Clad materials and powder fed methods	User industries
Turbine blade, shroud interlock	Triballoy/nimonics powder fed	Rolls Royce
Turbine blade, shroud interlock	PWA 694/nimonics preplace chips	Pratt & Whitney
Valve seat	Satellite 32, CrC_2, Cr, Ni, Mo/Cast Fe powder feed, preplaced powder	Toyota Fiat
Nuclear plant boiler tube	Co-based alloy preplaced chip	Ishikawa Heavy Industry
Turbine blade	Stellite 6 powder feed	GEC Alsthom
Turbine blade	Satellite, colmonoy preplaced, gravity feed	Westingshouse
Turbine blade	Stellite 6 powder feed	Japan Steel Corporation
Automotive	Cast iron system	General Motors
Aerospace	Stellite, T-800	Rockwell

cladding, depending upon the laser power density and powder feed rate. The powder precursor to be cladded or alloyed on the surface is either pre-placed in pre-determined thickness on the test surface followed by laser melting, or it may be fed through the powder feeder at various feed rates coupled with the laser beam. Various laser parameters, such as laser power, scan speed, and powder feed rate are optimized to achieve the preferred clad surface. However, large difference in thermal expansion coefficient of precursor and base substrate can cause cracking in the cladded layer.

7. Determination of Cavitation Erosion Resistance

Various methods have been employed to measure the cavitation erosion resistance of materials and coatings. A simple vibratory test method, documented as ASTM G32 (Ref 87), is the most widely used for generating the pure cavitation erosion data (Ref 10, 52, 57). In this method, a magnetostrictive or piezoelectric ultrasonic transducer is used to produce oscillations of test specimen in distilled water at a frequency of 20 ± 0.5 kHz. This is demonstrated by a schematic illustrated in Fig. 9. Transducer is connected to the horn (velocity transformer) to produce controlled oscillations. Monitoring of frequency and amplitude is made with a suitable calibrated device. A specimen of suitable dimension (diameter 15.9 ± 0.05 mm) is fitted at the other threaded end of the horn which is immersed in a beaker containing distilled water or appropriate experimental solution at 25 ± 2 °C. The minimum volume of liquid container should be around 2 L so that the liquid height can be maintained at ~100 mm and immersion depth of test sample at $\sim 12 \pm 4$ mm. The weights of specimen before and after the test are accurately measured to produce cumulative weight-loss data at fixed intervals. Specimen surface is prepared to a maximum surface roughness of ~0.8 μm. Final polishing up to 600 grit emery paper is sufficient, provided no visible pit or scratch is left on the surface. Such sites can otherwise serve as preferential/nucleation site for cavitation attack. The experimental solution and other parameters may be chosen to suit the purpose or to simulate the actual material-process conditions. Typical damage characteristic curves due to cavitation erosion shows three different stages. The incubation period during which internal stresses are accommodated in the outer surface without material loss, accelerative erosion resulting into significant mass loss as a result of cyclic impact load exceeding the fatigue limit of the material, and a steady-state mass loss. This is illustrated by a schematic in Fig. 10. Due to a nonlinearity in the cumulative mass-loss or mean depth of erosion (MDE) versus time curve (Fig. 10), comparison of erosion resistance of different alloys is difficult and needs careful evaluation. The erosion rate of a specific material should be reported with respect to maximum, terminal, and incubation rate/time as shown in Fig. 10.

Mechanism of cavitation erosion in vibratory facility is different as compared to that encountered by the hydraulic machinery (Ref 88). This difference is mainly due to the mode of bubble formation, development, and its implosion. In hydraulic machineries, cavitation is actually generated in the zones at low pressure of moving liquids (under vaporization pressure) while implosions take place in the zones of high pressure. In the vibratory facility, the bubble formation and implosion occurs at the same spot and therefore, it is more severe as compared to that in the hydraulic machineries. Also hydraulic machineries suffer from solid particle erosion in conjunction with the cavitation or combined cavitation-particle erosion damage.

Rotatory disk apparatus (RDA) has also been frequently used for accelerating the cavitation erosion (Ref 27, 58). Contrary to the vibratory horn (in ASTM G32), cavitation in RDA test method is generated in the flowing state of fluid, which actually resembles the underwater processes. It consists of a test chamber having disk of 340-mm diameter. The disk contains groves at a certain distance from the center where specimens are mounted. The brass cavity inducers are fixed near the specimens to generate bubbles in the water. Disk rotates at various speeds in water-filled chamber, during which cavitation occurs and causes erosion when bubble implodes. With RDA, cavitation and erosion can be determined independently or in combination of abrasive particles (Ref 27).

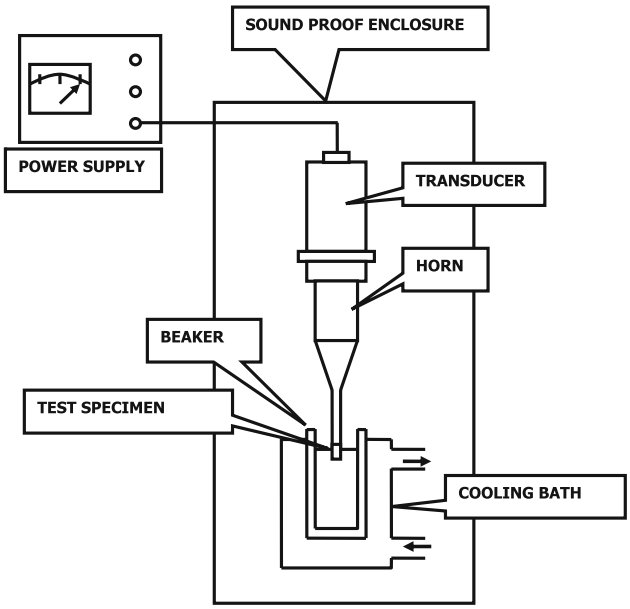

Fig. 9 Simple vibratory test method for cavitation erosion

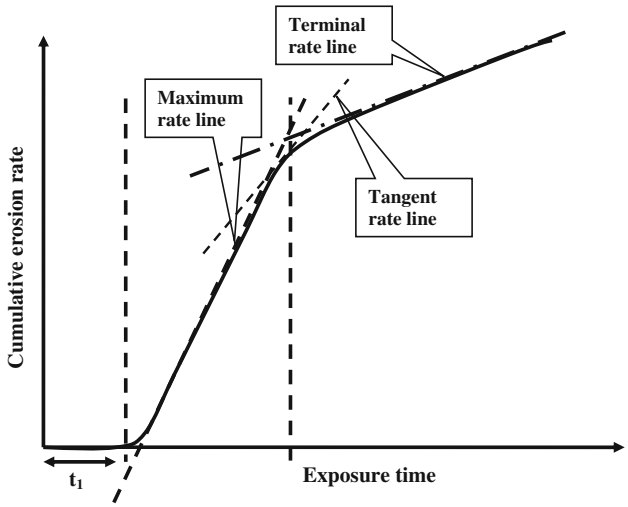

Fig. 10 Typical damage characteristic curves due to cavitation erosion

Another method of evaluating cavitation erosion is described in ASTM standard G134 (Ref 89) where cavitation is generated in flowing system and both the jet velocity as well as the downstream pressure can be varied independently. A pump capable of generating pressure ~21 MPa and flow rate ~4.5 L/min is generally used. In this method, test liquid is forced using a pump through the sharp nozzle in the form of jet at a constant pressure into the chamber. A specimen of a known initial weight is placed in the path of the jet at a certain distance from the nozzle. Standard test conditions generally include tap or deionized water at 35 ± 1 °C with corresponding vapor pressure ~0.00563 MPa. Apparatus is calibrated using standard reference materials at a fixed cavitation number (such as at σ ~0.014 and 0.025 with corresponding upstream and down stream pressures) depending upon the test material and duration. For this, upstream pressure may be specified and downstream pressure can be calculated from the Eq 1. The standoff distance from the nozzle is kept fixed for specimens to be compared. Upstream and downstream pressures in the chamber should be measured and monitored at regular intervals. The specimen is weighed before and after the test for every cycle, and cumulative weight loss versus time may be plotted as described in earlier test methods for erosion rate (Fig. 10). The data can be generated and compared for various engineering materials.

Liquid impingement erosion test, described in ASTM G73-04 (Ref 90), is often used for simulating the cavitation erosion. It can simulate the damage processes similar to that produced by repeated small-scale and high-intensity pressure pulses on the solid material surface. In this test, specimens are attached to the periphery of a rotating disk which passes through one or more liquid jets and sprays causing the discrete impacts. The rotating disk is generally fabricated for impact velocity ranging between 50 and 1000 m/s. At a very low velocity, corrosive effects of liquid may dominate, while at higher velocities, temperature of the specimen may increase and can influence the erosion rate. The jet (nozzle) diameter or droplets should uniformly fall (drops per unit volume) in the path traversed by specimen. The erosion rates are measured from the cumulative mass loss versus time curve during various interrupted cycles. It is generally recommended that the test should be continued until the erosion rate starts declining after the incubation time. The time interval between the two successive mass-loss measurements should be short enough to notice the incubation period and the maximum erosion rate. Under the controlled parameters, materials may be evaluated by determining the time to failure (end of useful service life) under simulated environment.

8. Summary and Future Direction

Cavitation erosion encounters by the hydroturbine components is the predominant damage mechanism that costs heavily to the hydropower industries. It is an extremely complex phenomenon which is yet to be fully understood, and research is in progress to unveil the details. The cavitation resistance of material seems to depend on the combination of material's properties, such as ultimate resilience, hardness, and toughness. Erodent size (such as silt), shape, hardness, and angle of impingement along with the hydrodynamic conditions are the parts of environment, which influence the cavitation of materials.

It is found out from the literature that the modification of hydrodynamic design and surface engineering are the main approaches adopted to overcome cavitation erosion problem. Research on the development of newer material for hydroturbine applications, however, is limited. The surface engineering including coating and microstructural modification has shown significant increase in the useful life of components. Industrially, limited coating compositions have been used for cavitation erosion resistance. However, several coating systems, such as carbides (e.g., WC-Cr_2C_3, and Cr_3C_2), cermets (e.g., 20CrC-80WC, 56W_2C/Ni/Cr, and 41WC/Ni/Cr/Co), oxides, and borides are under continued investigation at laboratories. Results show a varied success in offering the cavitation erosion resistance. IC, IMC with TiC reinforcement, and nitinol have also been suggested as another class of coatings. Nonmetals, particularly, elastomers (such as polyurethane) with the reinforced hard particles have often been used as coating material for the hydroturbine components. Thermal spraying, APS, and HVOF processes have been used commercially for applying coatings on the surface of actual components. CVD, PVD, and plasma nitriding are a few other methods which are being used in the laboratories, but their industrial application for large components is yet to be proven successful. Laser hardening and melting have shown promise to increase the cavitation erosion resistance by changing the microstructures and hardness of the outermost surface of component. Alternatively, the laser cladding with desired chemical composition (different from the substrate) on the surface could minimize the cavitation damage. The future study on the cavitation erosion needs to be focused on the following:

- Cavitation erosion is a complex phenomenon particularly in the presence of silt or erodent, and extensive study is required to develop fundamental understanding of the process. Extensive data would be needed on the cavitation erosion rates of various alloys of concern and for material development.
- Predictive capabilities to measure the cavitation intensities of the environments need to be investigated and established. The cavitation erosion resistance of various materials/components may subsequently be established against the environment of different cavitation intensities combined with the erodent.
- Coating has several physical interphases which are considered weak areas where mechanical and electrochemical failures may originate. Any coating/method that forms smooth and graded interphase would provide long-lasting solution against the cavitation erosion. The coating composition should be optimized so that the balance among hardness, toughness, and ductility can be achieved for high cavitation resistance. This should be investigated in detail before applying on the real components.
- The coatings applied on the hydroturbine components using commercially available methods, such as HVOF resulted in micro-cracking, disbonding, and the dig out of embedded ceramic particle. Possibility of the other coating methods such as laser cladding needs to be tried out and investigated as they produce metallurgically bonded coating. Such coatings may provide better stability under the loading impact.
- Newer composite coatings including nanocomposite of ternary and quaternary phases having combination of higher

hardness, strength, toughness, and adhesion should be studied for future applications. A combination of the soft and the hard phases can meet such complex demand.

Acknowledgments

The authors offer their sincere thanks to the Director, National Metallurgical Laboratory, Jamshedpur, for granting permission to publish this article. Help received from Shri Mukesh Kumar and Deepak Kumar in preparing the manuscript is sincerely acknowledged.

References

1. D. Whale and D. Hart, A Review of Cavitation-Erosion-resistant Weld Surfacing for Hydro Turbines, *Proceedings of the Asian-Pacific Welding Conference* (Auckland, New Zealand), 1996
2. G.I. Nikitenko, Studies to Reduce Cavitation Erosion of the Impellers in the Hydro Turbines at the Sayano-Shushenskoe Hydroelectric Plant, *Hydrotech. Constr.*, 1998, **32**(9), p 570–573
3. B.S.K. Naidu, Renovation and Modernization of Silt Prone Hydropower Stations in India, *Workshop on Silting Problems in Hydroelectric Power Stations*, June 25–26, 1987 (New Delhi), 1987, p 13–16
4. D.P. Sharma and S. Singh, Operational Problems of Water Turbine in U.P.—with Special Reference to Tiloth Power Station, *All India Seminar on Metallurgical Problems in Power Projects*, October 30–31, 1987 (Lucknow), 1987, p 18–35
5. B.S.K. Naidu, Silt Damages to Equipment in Hydro Power Stations and Remedial Measures, *CBIP Workshop*, July 25–26, 1996 (New Delhi), 1996
6. S.K. Singhal and S. Ratnendra, *Proceedings of the Himalayan Small Hydropower Summit*, Held During October 12–13, 2006 (Dehradun), 2006, p 200–207
7. M.K. Kesharwani, *Proceedings of the Himalayan Small Hydropower Summit*, Held During October 12–13, 2006 (Dehradun), 2006, p 44–57
8. P. Stelio. Renewable Energy in Canada Status Report 2002. A National Report Prepared for the Renewable Energy Working Party (REWP) of the International Energy Agency (IEA), Ontario, Canada, 2002, p 1–43
9. B.S. Mann, High Energy Particle Impact Wear Resistance of Hard Coatings and Their Application in Hydro Turbines, *Wear*, 2000, **237**, p 140–146
10. M. Duraiselvam, R. Galun, V. Wesling, B.L. Mordike, R. Reiter, and J. Oligmuller, Cavitation Erosion Resistance of AISI, 420 Martensitic Stainless Steel Laser-Clad with Nickel Aluminide Intermetallic Composites and Matrix Composite with TiC Reinforcement, *Surf. Coat. Technol.*, 2006, **201**, p 1289–1295
11. A. Karimi and J.L. Martin, Cavitation Erosion of Materials, *Int. Mater. Rev.*, 1986, **31**, p 1–26
12. K. Padhy Mamta and R.P. Saini, A Review on Silt Erosion in Hydro Turbines, *Renew. Sustain. Energy Rev.*, 2008, **12**, p 1974–1987
13. M.G. Fontana, *Corrosion Engineering*, McGraw Hill, Singapore, 1986, p 104
14. H. Brekke, Hydraulic Design of Turbines, *Abrasive Erosion and Corrosion of Hydraulic Machinery*, C.G. Duan and V.Y. Karelin, Ed., ICP, London, 2003,
15. W.S. Lamb, *Cavitation and Aeration in Hydraulic Systems*, BHR Group, Bedfordshire, 1987, p 114
16. R. Knapp, W. Daily, and F. Hammitt, *Cavitation*, McGraw-Hill, Singapore, 1970, p 578
17. C.M. Hansson and I.L.H. Hansson, ASM Handbook: Friction, *Lubr. Wear Technol.*, 1992, **18**, p 214–220
18. C.M. Preece, *Treatise on Materials Science and Technology, Volume 16, Erosion*, Academic Press Inc., New York, 1979, p 249–308
19. K. Timo, Cavitation in Fluid Power, *Proceedings of the 1st FPNI-PhD Symposium* (Hamburg), 2000, p 371–382
20. B. Vyas and C.M. Preece, Stress Produced in a Solid by Cavitation, *J. Appl. Phys.*, 1976, **47**, p 5133–5138
21. J.-H. Chen and W. Wu, Cavitation Erosion Behavior of Inconel 690 Alloy, *Mater. Sci. Eng. A*, 2008, **489**, p 451–456
22. H. Soyama and H. Kumano, The Fundamental Threshold Level—A New Parameter for Predicting Cavitation Resistance, *J. Test. Eval.*, 2002, **30**, p 421–431
23. Y. Iwai, T. Okada, and S. Tanaka, A Study of Cavitation Bubble Collapse Pressures and Erosion Part 2: Estimation of Erosion from the Distribution of Bubble Collapse Pressures, *Wear*, 1989, **133**, p 233–243
24. S. Hattori, T. Hirose, and K. Sugiyama, Prediction Method for Cavitation Erosion Based on Measurement of Bubble Collapse Impact Loads, *J. Phys. Conf. Ser.*, 2009, **147**, p 1–9
25. S. Hattori, B.H. Sun, F.G. Hammitt, and T. Okada, An Application of Bubble Collapse Pulse Height Spectra to Venture Cavitation Erosion of 1100 O Aluminum, *Wear*, 1985, **103**, p 119–131
26. S. Li, Cavitation Enhancement in Silt Erosion: Obstacles & Way Forward, *Fifth International Symposium on Cavitation (CAV2003)*, November 1–4, 2003 (Osaka, Japan), 2003, p 1–7
27. B. Thapa, P. Chaudhury, O.G. Dahlhaug, and P. Upadhyay, Study of Combined Effect of Sand Erosion and Cavitation in Hydraulic Turbines. *International Conference on Small Hydropower—Hydro Sri Lanka*, October 22–24, 2007, p 1–6
28. V.K. Nanda, Parameters Affecting Abrasion and Remedial Measures, *Proceedings of the 1st International Conference on Silting Problems in Hydro Power Plants* (New Delhi), 1999, p 43–52
29. M. Toshima, T. Okamura, J. Satoh, K. Usami, and S. Tanabe, Basic Study of Coupled Damage Caused by Silt Abrasion and Cavitation Erosion, *JSME B*, 1991, **57**, p 20–25
30. J.F. Santa, J.C. Baena, and A. Toro, Slurry Erosion of Thermal Spray Coatings and Stainless Steels for Hydraulic Machinery, *Wear*, 2007, **263**, p 258–264
31. I. Hussainova and I. Kleis, Investigation of Particle—Wall Impact Process, *Wear*, 1999, **233–235**, p 168–173
32. A. Ball and Z. Feng, The Erosion of Four Materials Using Seven Erodent—Toward an Understanding, *Wear*, 1999, **233–235**, p 674–684
33. S. Li, Cavitation Enhancement of Silt Erosion—An Envisaged Micro Model, *Wear*, 2006, **260**, p 1145–1150
34. G.F. Truscott, A Literature Survey on Abrasive Wear in Hydraulic Machinery, *Wear*, 1972, **20**, p 29–50
35. J. Zhang, M.O.W. Richardson, G.D. Wilcox, J. Min, and X. Wang, Assessment of Resistance of Non-Metallic Coatings to Silt Abrasion and Cavitation Erosion in a Rotating Disk Test Rig, *Wear*, 1996, **194**, p 149–155
36. J.C. Arnold and I.M. Hutchings, The Mechanisms of Erosion of Unfilled Elastomers by Solid Particle Impact, *Wear*, 1990, **138**, p 33–46
37. M. Bjordal, E. Bardal, T. Rogne, and T.G. Eggen, Erosion and Corrosion Properties of WC Coatings and Duplex Stainless Steel in Sand-Containing Synthetic Sea-Water, *Wear*, 1995, **186–187**, p 508–514
38. E. Bardal, *Korrosjon og korrosjonsvern*, Tapir, Trondheim, 1985 (in Norwegian)
39. N. Tsuguo, Estimation of Repair Cycle of Turbine due to Abrasion Caused by Suspended Sand and Determination of Desilting Basin Capacity, *Proceedings of the International Seminar on Sediment Handling Technique*, NHA, Kathmandu, 1999
40. S.C. Li, "Cavitation Damage: Three Gorge Turbines (Phenomenon, Implication & Unknowns…)," Presentations at the Three Gorge Power Station (19 March 2006), the Beijing University (28 March 2006) and the National Research Institute of Hydro Power (March 2006)
41. P. Linhardt and A. Nichtawitz, MIC in Hydroelectric Power Plants, *Corrosion 2003*, NACE International Houston, Texas, Paper No. 03564
42. R.J.K. Wood and J.A. Wharton, Investigation of Erosion-Corrosion Processes Using Electrochemical Noise Measurement, *Tribol. Int.*, 2002, **35**, p 631–641
43. M. Kjelsden, "Cavitation in Hydraulic Machinery," Dr. Ing. Thesis, NTNU, 1996, p 63
44. Y. Tetsuyuk, Anti-Erosion Materials for Hydroturbine, *Turbomachinery*, 2000, **28**, p 577–581
45. C.J. Heathcock, B.E. Protheroe, and A. Ball, Cavitation Erosion of Stainless Steels, *Wear*, 1982, **81**, p 311–327
46. K.Y. Chiu, F.T. Cheng, and H.C. Man, Laser Cladding of Austenitic Stainless Steel Using NiTi Strips for Resisting Cavitation Erosion, *Mater. Sci. Eng. A*, 2005, **402**, p 126–134
47. B.C.S. Rao and D.H. Buckley, Deformation and Erosion of F.C.C. Metals and Alloys Under Cavitation Attack, *Mater. Sci. Eng. A*, 1984, **67**, p 55

48. Z.D. Cui, H.C. Man, F.T. Cheng, and T.M. Yue, Cavitation Erosion-Corrosion Characteristics of Layer Surface Modified NiTi Shape Memory Alloy, *Surf. Coat. Technol.*, 2003, **162**, p 147–153
49. C.T. Kowk, F.T. Cheng, and H.C. Man, Laser Surface Modification of UNS S31603 Stainless Steel Using NiCrSiB Alloy for Enhancing Cavitation Erosion Resistance, *Surf. Coat. Technol*., 1998, **107**, p 31–40
50. N. Alonso-Falleiros, M. Magri, and I.G.S. Falleiros, Intergranular Corrosion in a Martensitic Stainless Steel Detected by Electrochemical Tests, *Corrosion*, 1999, **55**, p 769–778
51. F.J. Heymann, Toward Quantitative Prediction of Liquid Impact Erosion, *ASTM STP*, 1970, **474**, p 212
52. S. Hattori, R. Ishikura, and Q. Zhang, Construction of Database on Cavitation Erosion and Analyses of Carbon Steel Data, *Fifth International Symposium on Cavitation*, November 1–4, 2003 (Osaka, Japan), 2003
53. H. Niinaka, A. Hirose, and S. Sogabe, Hiroshi Noguchi: 13Cr-3.5 Martensitic Stainless Steel Casting for Hydraulic Turbine Runner. Kawasaki Steel Technical Report No. 14, March 1986, p 141–152
54. R. Garcia and F.G. Hammitt, Cavitation Damage and Correlation with Mechanical and Fluid Properties, *J. Basic Eng. D*, 1967, **89**, p 753–763
55. P. Veerabhadra Rao, C.S. Martin, B.C. Syamala Rao, and N.S. Lakshaman Rao, Estimation of Cavitation Erosion with Incubation Periods and Material Properties, *J. Test. Eval. A*, 1981, **9**, p 189–197
56. A. Thiruvengadam and S. Waring, Mechanical Properties of Metals and Cavitation Damage Resistance, *J. Ship Res.*, 1966, **10**, p 1–9
57. R.H. Richman and W.P. McNaughton, Correlation of Cavitation Erosion Behavior with Mechanical Properties of Metals, *Wear*, 1990, **14**, p 63–82
58. B.S. Mann, Boronizing of Cast Martensitic Chromium Nickel Stainless Steel and Its Abrasion and Cavitation-Erosion Behavior, *Wear*, 1997, **208**, p 125–131
59. K. Alicja and C. Andrzej, Cavitation Erosion Resistance of Cr-N Coating Deposited on Stainless Steel, *Wear*, 2006, **260**, p 1324–1332
60. J.Y. Ying, Ed., *Nanostructured Materials*, Academic Press, San Diego, 2001, p 168–198
61. R.W. Siegel and G.E. Fougere, Mechanical Properties of Nanophase Metals, *Nanostruct. Mater.*, 1995, **6**, p 205–216
62. H.S. Nalwa, Ed., *Handbook of Nanostructured Materials and Nanotechnology: Synthesis and Processing*, Vol 1, Academic Press, San Diego, 2000
63. R.J.K. Wood, Tribo-Corrosion of Coatings: A Review, *J. Phys. D Appl. Phys.*, 2007, **40**, p 5502–5521
64. V.A.D. Souza and A. Neville, Aspects of Microstructure on the Synergy and Overall Material Loss of Thermal Spray Coatings in Erosion-Corrosion Environments, *Wear*, 2007, **263**, p 339–346
65. D. Toma, W. Brandl, and G. Marginean, Wear and Corrosion Behaviour of Thermally Sprayed Cermet Coatings, *Surf. Coat. Technol.*, 2001, **138**, p 149–158
66. V.A.D. Souza and A. Neville, Linking Electrochemical Corrosion Behaviour and Corrosion Mechanisms of Thermal Spray Cermet Coatings (WC-CrNi and WC/CrC-CoCr), *Mater. Sci. Eng. A*, 2003, **352**, p 202–211
67. F.T. Cheng, C.T. Kwok, and H.C. Man, Laser Surfacing of S31603 Stainless Steel with Engineering Ceramics for Cavitation Erosion Resistance, *Surf. Coat. Technol.*, 2001, **139**, p 14–24
68. T. Chang, C.H. Yeh, J.L. He, and K.C. Chen, Cavitation Erosion and Corrosion Behavior of Ni-Al Intermetallic Coatings, *Wear*, 2003, **255**, p 162–169
69. H. Hiraga, T. Inoue, H. Shimura, and A. Matsunawa, Cavitation Erosion Mechanism of NiTi Coating Made by Laser Plasma Hybrid Spraying, *Wear*, 1999, **231**, p 272–278
70. D.H. Graham and A. Bell, Particle Erosion of Candidate Materials for Hydraulic Valves, *Wear*, 1989, **133**, p 125–132
71. E. Ness and R. Zibbell, Abrasion and Erosion of Hard Materials Related to Wear in the Abrasive Water Jet, *Wear*, 1996, **196**, p 120–125
72. B.S. Mann and A. Vivek, HVOF Coating and Surface Treatment for Enhancing Droplet Erosion Resistance of Steam Turbine Blades, *Wear*, 2003, **254**, p 652–667
73. K. Sugiyama, S. Nakahama, S. Hattori, and K. Nakano, Slurry Wear and Cavitation Erosion of Thermal-Sprayed Cermets, *Wear*, 2005, **258**, p 768–775
74. B.S. Mann and A. Vivek, Abrasive and Erosive Wear Characteristics of Plasma Nitriding and HVOF Coatings: Their Application in Hydro Turbines, *Wear*, 2001, **249**, p 354–360
75. P.W. Alexiff, Research and Development on Axial Fan Blade Erosion, *Combustion*, 1979, **7**, p 12–16
76. K.H. Lo, F.T. Cheng, and H.C. Man, Laser Transformation Hardening of AISI, 440C Martensitic Stainless Steel for Higher Cavitation Erosion Resistance, *Surf. Coat. Technol.*, 2003, **173**, p 96–104
77. C.T. Kwok, H.C. Man, and F.T. Cheng, Cavitation Erosion and Pitting Corrosion Behaviour of Laser Surface-Melted Martensitic Stainless Steel UNS S42000, *Surf. Coat. Technol.*, 2000, **126**, p 238–255
78. K. Venugopal and A. Manish, Application of High Power Lasers in Material Processing, *BHEL J.*, 2007, **28**(1), p 20–30
79. S. Basu, A.M. Sinnar, and G.S. Bohlander, *Measurement of Cavitation Resistance of Organic Marine Coatings, Mechanical Properties. Performance and Failure Modes of Coatings*, Cambridge University Press, Cambridge, 1984, p 85
80. R.J. Nuttall, The Selection of Abrasion Resistant Lining Materials, *Bulk Solids Handl.*, 1985, **5**, p 1041–1047
81. I.M. Kats, Investigation of the Cavitation Resistance of Elastic Polymer Coatings, *Power Technol. Eng.*, 1974, **8**, p 539–544
82. Y.P. Kathuria, Some Aspects of Laser Surface Cladding in the Turbine Industry, *Surf. Coat. Technol.*, 2000, **132**, p 262–269
83. L. Ahman, Microstructure and Its Effect on Toughness and Wear Resistance of Laser Surface Melted and Post Heat Treated High Speed Steel, *Metall. Trans. A*, 1984, **15**, p 1829–1835
84. P.A. Molian and M.J. Hsu, *Proceedings of Surface Modification Technologies*, I.S. Sudarshan and D.G. Bhat, Ed., The Materials Society, Warrendale, PA, 1988, p 155
85. J. Hu, Z. Li, Y. Wang, H. Wang, J. Lu, and L. Wang, *Trans. Met. Heat Treat.*, 1990, **2**, p 19–25
86. K. Toda, T. Mikami, and T. Hoshino, Effect of Ridge Around Dent and Retained Austenite on Rolling Fatigue Life, *J. Jpn. Inst. Met.*, 1994, **58**, p 1473–1478
87. "ASTM G32-03 Standard Test Method for Cavitation Erosion Using Vibratory Apparatus," ASTM Standards, Vol. 03.02, p 98–111
88. I. Bordeasu, M. Voda, V.A. Serban, and C. Codrean, Cavitation Erosion for G-X5crni13-14 Martensitic Stainless Steel with Various Heat Treatments, *The 6th International Conference on Hydraulic Machinery and Hydrodynamics Timisoara*, October 21–22, 2004 (Romania), 2004
89. "ASTM G134-03 Standard Test Method for Erosion of Solid Materials by a Cavitating Liquid Jet," ASTM Standards, Vol. 03.02, p 559–571
90. "ASTM G73-04 Standard Practice for Liquid Impingement Erosion Testing," ASTM Standards, Vol. 03.02, p 273–290